


RESEARCH

Open Access



Photothermal therapy combined with a STING agonist induces pyroptosis, and gasdermin D could be a new biomarker for guiding the treatment of pancreatic cancer

Yanyan Hu^{1†}, ErPeng Qi^{2†}, Chao Yun^{1,3†}, Xi Li^{4†}, Fangyi Liu², Zhigang Cheng², Na Guan^{1,3}, Qiong Wang⁵, Huixia Zhao¹, Wenhua Xiao¹, Liang Peng¹, Jingwen Yang^{1*}  and Xiaoling Yu^{2*}

Abstract

Purpose Although photothermal therapy (PTT) can induce antitumour immunity, the mechanisms underlying its effects in pancreatic cancer (PC) require further exploration. In this study, the mechanism of action of PTT and its connection to pyroptosis as well as the therapeutic potential of PTT alone and in combination with STING agonists, were investigated. In addition, a biomarker of PC was found to stratify patients who are suitable for PTT.

Experimental design We explored whether PTT can induce pyroptosis in vitro and evaluated the therapeutic efficacy and antitumour immunity-inducing ability of PTT combined with STING agonist (c-di-GMP) as immune adjuvant in vivo in PC. We also evaluated gasdermin D (GSDMD) expression in tumour tissues and investigated drug sensitivity in patient-derived organoids (PDOs) with differential GSDMD expression.

Results Our study demonstrated that local PTT induces pyroptosis via the caspase-1/GSDMD pathway and elicits antitumour immunity. PTT combined with a STING agonist exhibits better therapeutic efficacy than PTT alone while limiting distant tumour metastasis, and enhances the immune response by promoting dendritic cell maturation, increasing the frequency of tumour infiltrating T cells, and converting macrophages from the M2 to the M1 phenotype. In addition, we found that GSDMD is highly expressed in tumour tissues and that overexpression of GSDMD in PC might suggest increased resistance to chemotherapy and the potential benefits of local therapy. We further confirmed that PDOs with higher GSDMD expression are less sensitive to a chemotherapeutic agent (5-Fluorouracil) than PDOs with lower GSDMD expression, making GSDMD a new biomarker for identifying patients who may benefit from PTT.

[†]Yanyan Hu, ErPeng Qi, Chao Yun and Xi Li contributed equally to this work.

*Correspondence:
Jingwen Yang
8537505@sina.com
Xiaoling Yu
dyuxl301@aliyun.com

Full list of author information is available at the end of the article



© The Author(s) 2025. **Open Access** This article is licensed under a Creative Commons Attribution-NonCommercial-NoDerivatives 4.0 International License, which permits any non-commercial use, sharing, distribution and reproduction in any medium or format, as long as you give appropriate credit to the original author(s) and the source, provide a link to the Creative Commons licence, and indicate if you modified the licensed material. You do not have permission under this licence to share adapted material derived from this article or parts of it. The images or other third party material in this article are included in the article's Creative Commons licence, unless indicated otherwise in a credit line to the material. If material is not included in the article's Creative Commons licence and your intended use is not permitted by statutory regulation or exceeds the permitted use, you will need to obtain permission directly from the copyright holder. To view a copy of this licence, visit <http://creativecommons.org/licenses/by-nc-nd/4.0/>.

Conclusions In this work, c-di-GMP was used as an immune adjuvant for PTT to treat PC for the first time, and the results provide clues for the development of novel combination immunotherapies that simultaneously suppress primary tumours and distant metastases. GSDMD has great potential as a new biomarker for the selection of individualized treatment modalities.

Keywords Pyroptosis, Photothermal therapy, Pancreatic cancer, STING agonist, GSDMD

Introduction

Pancreatic cancer (PC) is one of the most lethal malignancies, with a five-year survival rate of less than 10% [1]. Despite modern advances in diagnosis, surgical, and medical therapies, PC has an extremely poor prognosis owing to its unique immunosuppressive tumour micro-environment (TME) and natural resistance to conventional radiotherapy, chemotherapy, etc [2, 3]. Recently, some progress in the treatment of PC has been made, including the use of immune checkpoint inhibitors (ICIs), adoptive T-cell therapy (ACT) and tumour vaccines [4–6]. However, for PC patients with high microsatellite instability (MSI-H), the objective response rate (ORR) was only 18.2% in the single-arm KEYNOTE-158 trial, which was substantially lower than the response rates reported for patients with MSI-H cholangiocarcinoma (40.9%) and small intestine (42.1%), gastric (45.8%), and endometrial (57.1%) cancers [7, 8]. In addition, owing to difficulties in large-scale manufacturing and standardization, the application of cancer vaccines and ACT is limited [9–11].

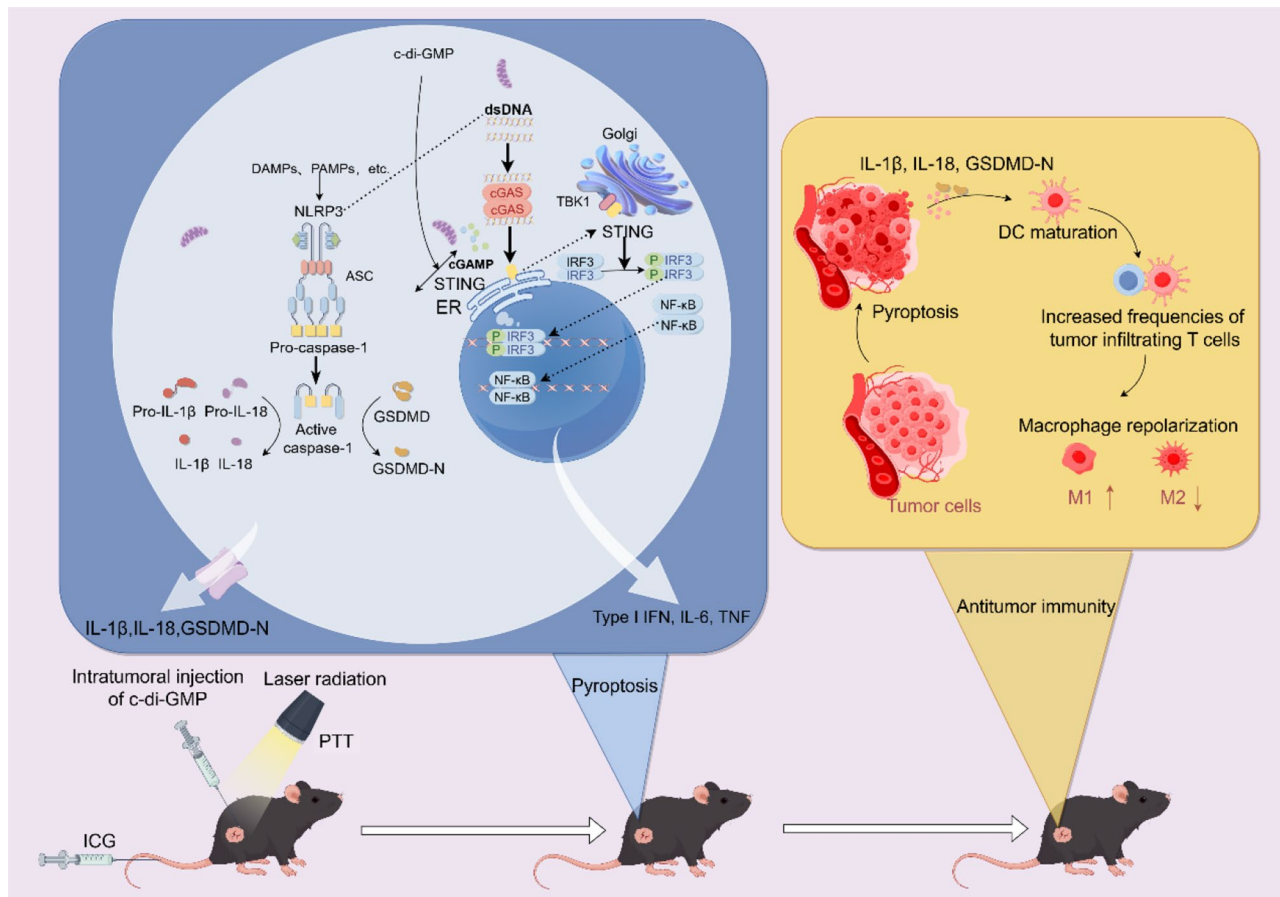
Photothermal therapy (PTT) is a promising strategy for cancer treatment with a short time of action, few adverse effects, and good therapeutic effectiveness that causes minimal damage to normal tissues [12]. On the basis of our previous study, PTT is a minimally invasive therapy that can efficiently eradicate pancreatic tumours [13]. Several studies have reported that PTT can control primary tumours and metastases [14], possibly through the induction of immunogenic cell death (ICD) of tumour cells, the release of tumour antigens, and the subsequent augmentation of antitumour immune responses [15, 16].

Pyroptosis is a type of proinflammatory programmed cell death that has attracted increased interest in relation to tumour therapies in recent years [17–19]. It is characterized by cell swelling, pore formation on the plasma membrane and the release of cellular contents, such as inflammatory factors, tumor-associated antigens (TAAs) and damage-associated molecular patterns (DAMPs), which increases immunogenicity to activate tumour-specific adaptive immunity [20, 21]. Pyroptosis can be triggered by inflammasome activation via various influencing factors, such as pathogen-associated molecular patterns (PAMPs) and DAMPs [22, 23]. The inflammasome is a multimeric complex composed of essential components that can activate caspase family proteins to cause various physiological reactions [17, 24–26]. Gasdermins, which

are pore-forming effector proteins, are effectors of pyroptosis [27, 28]. Recent studies have demonstrated that pyroptosis can be activated mainly by the canonical caspase-1/gasdermin-D (GSDMD) pathway, the noncanonical caspase-4/5/11/GSDMD inflammatory pathway, or the caspase-3/ gasdermin E (GSDME) pathway [24, 29].

Pyroptosis is induced by the inflammasome which is usually formed by sensor proteins called pattern-recognition receptors (PRRs), an adaptor protein (ASC) called apoptosis-associated speck-like protein containing a caspase recruitment domain (CARD), and an inactive procaspase-1 molecule [20, 30, 31]. There are five main types of inflammasomes involved in canonical pathways: the NOD-like receptor protein 3 (NLRP3) inflammasome, the AIM2 inflammasome, the NLRP1 inflammasome, the PYRIN inflammasome, and the NLRC4 inflammasome [32, 33]. When PRRs are stimulated, the NLRP3 inflammasome, the most common inflammasome, can be activated by bacterial, viral, and endogenous DAMPs, produce mature caspase-1 and lead to GSDMD cleavage [34, 35]. Activated caspase-1/11 can cleave complete GSDMD into two parts, namely, GSDMD-NT (the N-terminal domain of GSDMD) and GSDMD-CT (the C-terminal domain of GSDMD), but only caspase-1 is able to activate IL-1 β and IL-18 [36, 37] (Schematic 1). Pyroptosis is also a type of ICD that can markedly increase anti-tumour immunity [38, 39]. To date, whether PTT can induce pyroptosis in PC and whether PTT induces cancer immunotherapy via pyroptosis have rarely been analysed, prompting us to explore the association between PTT and pyroptosis.

Activation of the cyclic-GMP-AMP synthase (cGAS)-stimulator of interferon gene (STING) pathway has been shown to have great potential as a target for cancer immunotherapy [40, 41]. DNA damage, chromosome instability, and oncosuppressor gene mutation and deletion in cancer cells lead to the accumulation of cytoplasmic DNA, which is recognized by cGAS. cGAS is activated through direct binding to double-stranded DNA (dsDNA), facilitating the synthesis of 2'-3'-cGAMP and inducing the activation of STING. Activated STING then recruits TANK binding kinase 1 (TBK1), which phosphorylates IFN regulatory factor 3 (IRF3) to initiate type I interferon (IFN-I) responses, while also promoting nuclear factor κ B (NF- κ B)-driven inflammatory cytokine release [42, 43] (Schematic1). Multiple studies have shown that the activation of cGAS-STING pathway



Scheme 1 A schematic summary of this study, showing that PTT induces pyroptosis via caspase-1/GSDMD pathway and arouses antitumour immune response. PTT combined with a STING agonist (c-di-GMP) as an immune adjuvant can amplify the aroused antitumour immunity

promotes the maturation of dendritic cells (DCs), facilitates antigen presentation to CD4⁺ T cells and increases the frequency of tumour-specific CD8⁺ T cells [44–47]. Therefore, the activation of STING, an intracellular receptor residing in the endoplasmic reticulum, has shown great potential for enhancing antitumour immunity through the induction of a variety of proinflammatory cytokines and chemokines [48]. Recently, several studies have shown that there are connections between the cGAS-STING pathway and the pyroptosis pathway and that increased STING signalling can promote NLRP3 inflammasome-mediated pyroptosis [49, 50]. Therefore, we are the first to propose the use of PTT combined with a STING agonist as a treatment for PC with enhanced efficacy.

Several natural and synthetic STING agonists have been developed and tested for their ability to treat cancers or infectious diseases in preclinical models and in the clinic [51]. Cyclic dinucleotides (CDNs), such as cyclic dimeric guanosine monophosphate (c-di-GMP), belong to a class of STING agonists that can trigger potent immune responses [52]. However, natural CDNs are susceptible to enzymatic degradation at low concentrations

in target tissues and have narrow therapeutic windows [40]. The combination of STING agonists with other therapies or the use of novel delivery systems for STING agonists may address these challenges.

In this study, we investigated whether PTT can induce pyroptosis and elicit antitumour immunity. We also evaluated the therapeutic efficacy and antitumour immunity-inducing ability of PTT combined with a STING agonist (c-di-GMP) as an immune adjuvant *in vivo*. Our findings demonstrated that PTT using indocyanine green (ICG) as a photothermal agent induced PC cell pyroptosis via the GSDMD-dependent canonical inflammasome pathway *in vitro* and *in vivo*. Local PTT reinvigorated antitumour immunity by increasing the frequency of mature DCs and CD8⁺ and CD4⁺ T cells in a subcutaneous xenograft model and inhibited distant tumours in a synergistic bilateral tumour model. Compared with PTT alone, PTT in combination with the STING agonist exhibited increased therapeutic efficacy, yielding favourable survival, and boosted the immune response by promoting the maturation of DCs and initiating T-cell clone expansion (Schematic1). Moreover, PTT altered the TME by converting macrophages from the M2 phenotype to the

M1 phenotype and depleting both collagen and cancer-associated fibroblasts (CAFs) in tumours. GSDMD was found to be highly expressed in PC tissues, and overexpression of GSDMD was found to suggest increased resistance to chemotherapy and the potential benefits of local therapy, such as PTT. Therefore, GSDMD can serve as a promising biomarker for selecting local therapy or chemotherapy for treating PC. In conclusion, our studies provide evidence for the efficacy of STING agonists as immune adjuvants for PTT and suggest that PTT combined with a STING agonist may be beneficial for treating PC, particularly for patients with GSDMD overexpression.

Methods

Cell lines

The mouse pancreatic carcinoma cell line Pan02-luc, labeled with luciferase using a standard stable transfection protocol, was purchased from IMMOCELL (Xiamen, Fujian, China) and cultured in Dulbecco's modified Eagle medium (DMEM; 11965092, Gibco). The human pancreatic adenocarcinoma cell line SW-1990-LUC labeled with luciferase, was purchased from Xuanyi Biotechnology Service Center (Shanghai, China) and cultured in RPMI-1640 medium (8122269, Gibco). The cell lines were cultured with 10% fetal bovine serum (FBS; 10099141, Gibco) and 1% penicillin/streptomycin (15140122, Gibco) at 37 °C in a 5% CO₂ atmosphere.

In vitro photothermal therapy

Indocyanine green (ICG, Dandong Yichuang Pharmaceutical Co., LTD, China) was selected as the photothermal sensitizer for PTT, which has already been approved by FDA in clinical use as its good performance on biological safety. And 808 nm laser source (MDL-H-808 nm-2 W-13040029, Changchun New Industries Optoelectronics Tec. Co., Ltd., China) was used to perform PTT with the output power density set to 1 W cm⁻². The cells in ICG and PTT group were incubated with ICG (100 µg mL⁻¹) for 6 h at 37 °C. The wells were washed three times with PBS and added with normal culture medium before irradiated with or without NIR laser for 5 min (λ = 808 nm, 1 W cm⁻²).

Cell morphology

To examine cell morphology, time-lapse cell changes were visualized using an optical microscope (CKX53SE, OLYMPUS) at 5, 25, and 45 min after PTT. The balloon-like cells were considered as pyroptotic cells. VX-765 (S2228, Belnacasan, Selleck), a caspase-1 selective inhibitor, was used 2 h prior to PTT. The shown images are representative of at least three randomly selected fields of view. Pyroptosis index of each field of view was calculated

as the ratio of the pyroptotic cell number to the total cell number in a snapshot multiplied by 100.

LDH release assay

Cells were seeded in 48-well plates and PTT was performed. Culture supernatants were collected 1 h post PTT and the LDH release was detected using LDH Cytotoxicity Assay Kit (C0016, Beyotime Biotechnology, China). Briefly, the supernatants were transferred into a 96-well plate and added with LDH detection reagents. The plates were then incubated for 30 min at room temperature in the dark. The absorbance value at 490 nm was measured and 630 nm was used as the reference wavelength. The LDH release rate was calculated as follows: $(\text{LDH}_{\text{sample}} - \text{LDH}_{\text{background}}) / (\text{LDH}_{\text{maximum}} - \text{LDH}_{\text{background}}) \times 100\%$, in which LDH_{sample}, LDH_{background} and LDH_{maximum} indicated LDH release of cells after PTT, untreated cells and cells treated with lysis solution, respectively.

Western blotting

Cells were washed with cold PBS and lysed in IP bufer (20 mM pH 7.5 Tris, 150 mM NaCl, 1% Triton X-100) supplemented with Protease Inhibitor Cocktail (Beyotime Biotechnology, China). Total proteins of cells were extracted and the protein concentration was determined by BCA assay (P0012, Beyotime Biotechnology, China). Equal amount of proteins were separated by SDS-PAGE, transferred to PVDF membranes (Millipore, Billerica, MA, USA), and probed with anti-DFNA5/GSDME antibody (1:1000, ab215191, Abcam, Cambridge, CB2 0AX, UK), anti-caspase-3 antibody (1:1000, 9662, Cell Signaling Technology, Danvers, MA, USA), anti-GSDMD antibody (1:1000, YT7991, Immunoway Biotechnology, Plano, TX, USA), anti-caspase-1 antibody (1:1000, 2225, Cell Signaling Technology), anti-p-IRF3 antibody (1:1000, 4947, CST) and anti-β-Actin antibody (1:1000, HX1827, huaxingbio, China). HRP-conjugated secondary antibodies recognizing mouse and rabbit IgG were used at 1:5000. Immunoblots were developed using ECL reaction system and gel-imaging system (Tanon, China).

Enzyme-linked immunosorbent assay (ELISA)

The release of mature IL-1β and IL-18 in the culture supernatants of cell lines was determined using IL-1β ELISA kit (EH001) and IL-18 ELISA kit (EH047), both of which were purchased from ExCell Bio (Shanghai, China). The procedures were carried out according to the manufacturer's instructions. The absorbance was measured using a microplate reader (Bio-Rad Laboratories, USA) at a wavelength of 450 nm and a correction at 655 nm.

Animals

Male BALB/c nu/nu mice and C57BL/6 N mice aged five-week were purchased from Charles River Laboratories (Beijing, China), and housed with standard temperature and humidity, as well as a regular 12 h light/12 h dark cycle. Food and water were provided ad libitum at all time. All animal experiments were approved by the Animal Ethics Committee of Chinese PLA General Hospital and were carried out in compliance with the Animal Management Rules of the Ministry of Health of the People's Republic of China (Document NO.55, 2001).

Evaluation of antitumour effect upon treatment of PTT *in vivo*

For evaluation of anti-tumour effect, BALB/c nu/nu mice were injected subcutaneously with 2×10^6 SW-1990-LUC cells suspended in 100 μ L PBS per mouse. About 10 days later, when the length of the tumour reached 5 mm, the mice were randomly divided into three groups (Blank, ICG and PTT group). Mice in the ICG and PTT groups were injected with ICG (100 μ g mL⁻¹, 100 μ L) and mice in the PTT group received PTT treatment (λ =808 nm, 42–48 °C, 8 min) 4 h post injection. All mice were sacrificed at 4–6 h after PTT and the tumour tissues were excised. H&E staining of tumour tissues were performed to assess the anti-tumour efficiency of PTT. The therapeutic effect of each therapy was monitored and 3 mice were sacrificed in each group at day 0, 3, 6, 9, 12 and 15 post treatment. The primary tumours were obtained and the tumour weights were measured every 3 days. For survival analysis, the mice were divided into three groups (n =5; Blank, ICG and PTT group) and monitored for 60 days. For biosafety analysis, the body weight of each mouse was measured using an electronic balance every 3 days.

Evaluation of synergistic therapeutic effect of PTT combined with a STING agonist

For further evaluation of the therapeutic effect of PTT combined with STING agonist c-di-GMP (HY-110382, MedChemExpress, NJ, USA), C57BL/6 N mice were injected subcutaneously with 5×10^6 Pan02-luc cells per mouse. The animal models were ready for experiments in approximately 7–10 days when the xenografted pancreatic tumour length reached 5 mm. The mice were divided into five groups (Blank, ICG, PTT, c-di-GMP and c-di-GMP+PTT group). In the ICG, PTT and c-di-GMP+PTT groups, mice were injected with ICG (100 μ g mL⁻¹, 100 μ L) via tail vein. In the PTT and c-di-GMP+PTT groups, mice received PTT treatment (42–48 °C, 8 min) 4 h post injection at day 0 and day 2. In the c-di-GMP and c-di-GMP+PTT groups, intratumoural injection of c-di-GMP (200 μ g mL⁻¹, 50 μ L, HY-110382, MedChemExpress, USA) was carried out at day 0 and day 2. The body weight and tumour size were measured every

2 days. The tumour volume was calculated according to the following formula: width² \times length \times 0.5. For survival analysis, mice were monitored for 90 days. Major organs (heart, liver, spleen, lung, kidney, stomach, intestine and brain) were fixed in 4% paraformaldehyde for H&E staining to assess the biocompatibility of combination therapy 14 days post-treatment.

Antitumour immune response induced by PTT and the combination therapy *in vivo*

To further evaluate the antitumour immunity and inhibitory effect on distant metastases by PTT alone and the combination therapy, a synergistic bilateral tumour model was established. C57BL/6 N mice were injected subcutaneously with 5×10^6 and 1×10^6 Pan02-luc cells onto the right and left flanks to imitate primary and distant tumours, respectively. The animal models were ready for experiments in approximately 7–10 days when the xenografted pancreatic tumour length reached 5 mm on the right flank. The mice were divided into four groups (Blank, PTT, c-di-GMP and c-di-GMP+PTT group). At day 7 post-treatment, the blood, the primary and distant tumours, and major organs were harvested for flow cytometry, immunofluorescence staining and H&E staining. The body weight and tumour size were measured every 2 days. For survival analysis, mice were monitored for 90 days.

Analysis of data accessed from the TCGA, GTEx and GDSC databases

The RNA sequencing (RNA-seq) data of 178 tumour samples of PC and 167 normal pancreatic samples with their clinicopathological parameters were downloaded from the cancer genome atlas (TCGA, <https://portal.gdc.cancer.gov>) and Genotype-Tissue Expression (GTEx, <https://www.gtexportal.org/home/>) databases. Drug resistance analysis was performed using data accessed from the latest version (GDSC2) of GDSC database. The cell line gene expression profile data were also acquired (<https://www.cancerrxgene.org/>). Using the R package “ggpubr”, the correlation between the expression of the GSDMD in PC cell lines and the response to the chemotherapeutics (5-Fluorouracil, Irinotecan, Paclitaxel, Cisplatin, and Gemcitabine) was visualized, and the Pearson's correlation coefficients were calculated. Samples between the GSDMD high- and low- expression groups were analysed for immune infiltration using the CIBERSORT package. Samples were screened based on a p-values of less than 0.05 and Wilcoxon was used to compare the difference in infiltration of significantly infiltrating immune cells between the two groups. The “estimate” package was used to perform an estimated analysis on the high- and low-expression groups of GSDMD, and the “ggplot2” package was used to draw violin diagrams using the Wilcoxon

test. Correlations between GSDMD gene and immune microenvironment score were further calculated using Spearman's test and Mantel's test.

Human specimens

20 pairs of PC tumor and pancreatic samples were obtained from patients undergoing surgery at the Chinese PLA General Hospital for detection of GSDMD expression by IHC. All the samples were confirmed as tumour or normal tissues based on pathologist assessment. And studies involving human samples were conducted in accordance to recognized ethical guidelines (Declaration of Helsinki) and approved by the Ethics Committee of the Fourth Medical Center of Chinese PLA General Hospital (Document NO. 2024KY045-KS001) with written informed consent.

Establishment of patient-derived organoid (PDO)

The tumour tissues were immersed immediately in transfer media at 4 °C post-dissection. After thorough washing with irrigation buffer (KS100121, Daxiang Biotech), the cleaned tissue was finely minced and combined with dissociation reagent (KS100123, Daxiang Biotech). Subsequent to digestion, cells were harvested, suspended and filtered. The resulting filtrate underwent centrifugation to collect cells, which were then resuspended in pancreatic cancer organoid culture medium (OC100138, Daxiang Biotech) and 3D matrigel (DatrixGel™, Daxiang Biotech). This cell suspension was seeded into a 24-well plate for subsequent organoid culture. All organoid models were routinely tested for Mycoplasma. Besides, H&E staining and IHC were performed using tumour tissues and PDOs for authentication. Tumour tissues with differential expression of GSDMD were used to conduct PDOs, which were named as PDO A and PDO B.

Drug response analysis of PDO

The PDO A and PDO B organoids were embedded in Matrigel and cultured. During the logarithmic growth phase, the organoids were dissociated into single cells, mixed with Matrigel, and seeded into IBAC S1 plates at the density of 1000 cells/well. 100 µL of PC organoid culture medium was then added to each well, and the cells were cultured for 3 days. Following the incubation period, the medium was gently removed and refilled with 150 µL of fresh medium with different concentrations of the tested drug. Each condition was conducted in triplicate, with corresponding blank wells (medium without cells), as well as negative and positive control (Staurosporine, MCE) wells. After 4 days of drug incubation, the CellCounting-Lite 3D Luminescent Cell Viability Assay (Vazyme, DD1102-03) solution was mixed with DMEM/F-12 basal medium at a 1:1 ratio as the detection reagent. The luminescence intensity was measured

using a fixed gain setting of 135, and the raw data were recorded. The cell inhibition rate was calculated using the following formula: Inhibition Rate (%) = [(RLU value of negative control - RLU value of treated sample) / (RLU value of negative control - RLU value of blank well)] × 100%. The concentration-response curve was plotted, and the half-maximal inhibitory concentration (IC₅₀) was calculated using GraphPad Prism 8.0.

Flow cytometry analysis

Flow cytometry analysis was performed using fresh tissues. For sample preparation, tumours and spleen tissues were dissociated into single cell suspension and resuspended in binding buffer. For detection of DC maturation, cells derived from spleens were stained with antibodies against CD45 (147710, BioLegend, San Diego, CA, USA), CD11c (117328, BioLegend), CD80 (104708, BioLegend) and CD86 (105032, BioLegend). For assay of T cells, cells were stained with antibodies against CD45 (147710, BioLegend), CD3 (100206, BioLegend), CD4 (100443, BioLegend), CD8 (100722, BioLegend), CD25 (102007, BioLegend) and Foxp3 (17-5773-82, Thermo Fisher, Waltham, MA, USA). The stained cells were then analysed with a flow cytometer (BD Biosciences, CA, USA). The matured DCs were defined as CD45⁺CD11c⁺CD86⁺. CD4⁺, CD8⁺ and Treg cells were defined as CD45⁺CD3⁺CD4⁺, CD45⁺CD3⁺CD8⁺ and CD45⁺CD4⁺CD25⁺Foxp3⁺, respectively.

Immunohistochemical analysis

For immunohistochemical staining of tumour tissues and PDOs, the sections were deparaffinized, rehydrated and incubated in sodium citrate buffer for antigen retrieval. Then 1% H₂O₂ was used to suppress the activity of endogenous peroxidase. Thereafter, the sections were incubated with primary antibodies at 4 °C overnight. Antibodies used included anti-cleaved caspase-1 antibody (386826, United States Biological, Marblehead, MA, USA), anti-IL-18 antibody (abx109929, Abbexa, Cambridgeshire, UK), anti-IL-1β antibody (83186, Cell Signaling Technology) and GSDMD antibody (Proteintech, Rosemont, IL, USA). The sections were then incubated with HRP-conjugated secondary antibodies for 1 h at room temperature. Finally, immunospecific reactivity was visualized by diaminobenzidine (DAB; ZSGB-BIO, Beijing, China) substrate and the sections were counterstained with hematoxylin (Jiancheng Biotech, Nanjing, China). Images were captured under a digital scanner (NanoZoomer 2.0, Hamamatsu, Japan).

Immunofluorescence staining

Immunofluorescence staining was performed on paraffin sections prepared as described in "Histological and immunohistochemical analysis" section. After

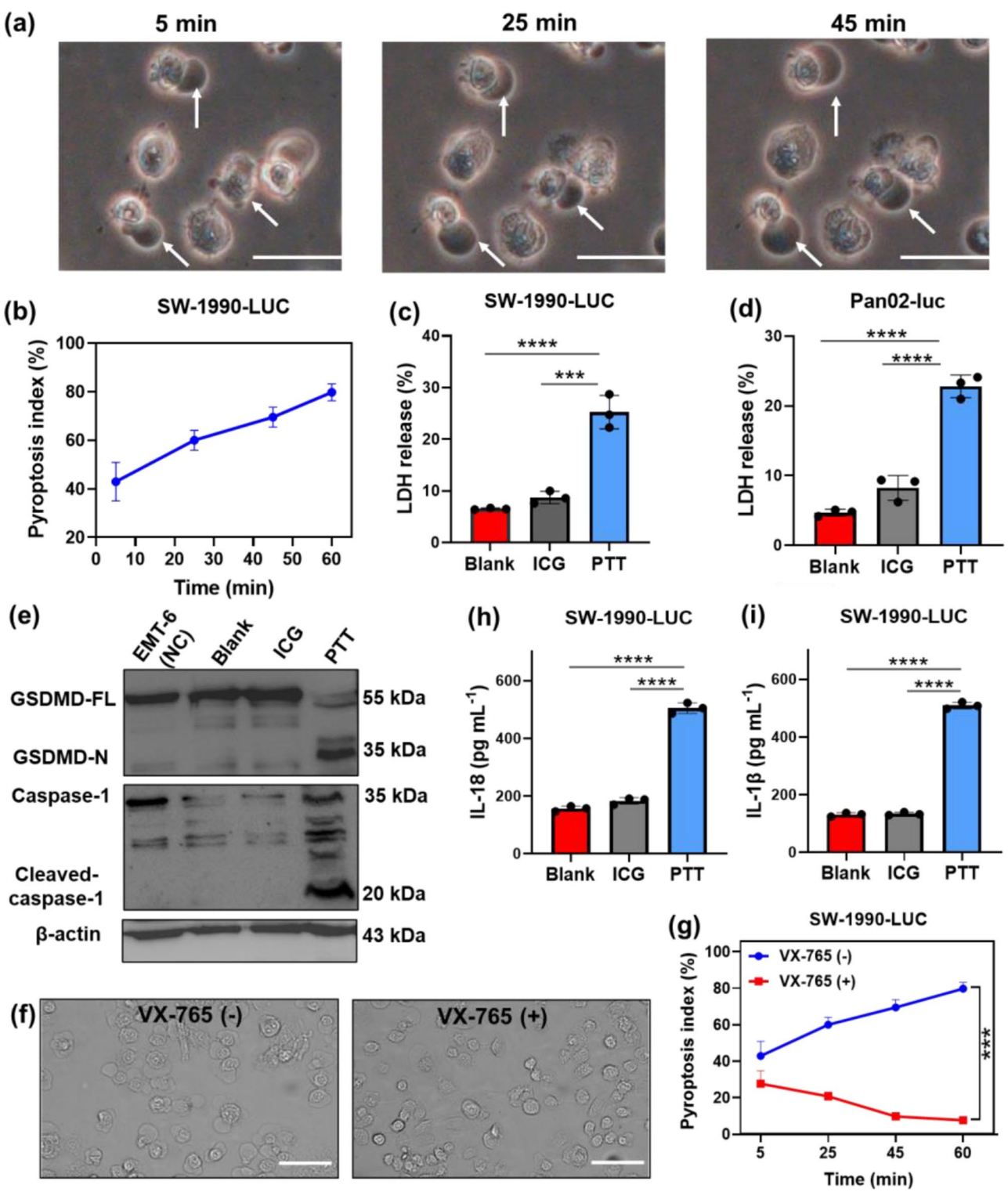


Fig. 1 (See legend on next page.)

deparaffinization, rehydration and antigen retrieval, the sections were permeabilized with 0.2% Triton X-100 and incubated in 5% BSA solution. Then the sections were incubated with primary antibody against cleaved-GSDMD (36425, Cell Signaling Technology) at 4 °C overnight. After that, secondary antibodies conjugated with Alexa Fluor 488, as well as 4, 6-diamidino-2-phenylindole (DAPI), were used in turn. Images were

(See figure on previous page.)

Fig. 1 Pyroptosis triggered by PTT via the caspase-1/GSDMD pathway in PC cell lines. **(a)** Real-time morphological tracking of SW-1990-LUC cells after PTT under a bright field microscope. Cells were treated with ICG at $100 \mu\text{g mL}^{-1}$ and irradiated for 5 min at 1 W cm^{-2} . White arrowheads indicate ballooned cell membrane which is the characteristic of pyroptotic cells. Scale bar: $100 \mu\text{m}$. **(b)** Pyroptosis index of SW-1990-LUC cells at different time points after PTT. **(c and d)** Cytotoxicity of PTT measured by LDH release in SW-1990-LUC and Pan02-luc cells. **(e)** Expression and cleavage of GSDMD and caspase-1 in SW-1990-LUC cells. Total proteins were extracted and subjected to western blotting analysis. Total proteins of breast cancer cell line EMT-6 were used as a negative control. **(f and g)** The morphology and pyroptosis index of SW-1990-LUC cells after PTT with or without VX-765 (a caspase-1 selective inhibitor) pre-treatment. Scale bar: $100 \mu\text{m}$. **(h and i)** IL-18 and IL-1 β release of SW-1990-LUC cells in different groups. Data were represented as mean \pm SD ($n=3$) if they accord with normal distribution. The comparison among different groups was carried out using one-way ANOVA followed by post hoc test. ***, $P<0.001$; ****, $P<0.0001$

captured under a digital scanner (NanoZoomer 2.0, Hamamatsu, Japan). To evaluate the M1/M2 macrophages polarization, collagen density and α -SMA, primary and distant tumours from C57BL/6 N mice were collected and subsequently frozen. Antibodies against α -SMA (GB12045, Servicebio), collagen (GB11022-3, Servicebio), F4/80 (GB113373, Servicebio), iNOS (GB1119, Servicebio) and CD206 (GB113497, Servicebio) were used.

Statistical analysis

All experiments were repeated for at least three times independently. PRISM 5.0 (GraphPad Software, San Diego, CA) was used for statistical analysis and graph production. Data were represented as mean \pm SD if they accord with normal distribution. The comparison among different groups was carried out using two-tailed t-test or one-way ANOVA followed by post hoc test. For survival analysis, Kaplan-Meier survival curves were conducted and the comparison between different groups was performed by Mantel-Cox test. $P<0.05$ was considered statistically significant.

Results

PTT induces pyroptosis via caspase-1/GSDMD pathway

To investigate whether pyroptosis can be induced by PTT, SW-1990-LUC and Pan02-luc cells treated with ICG were irradiated with near-infrared (NIR) light (808 nm). We explored the conditions of PTT, and the temperature curves corresponding to different concentrations of ICG are shown in Fig. S1. The results showed that the temperature could be maintained between 42°C and 48°C when the concentration of the ICG solution was $100 \mu\text{g mL}^{-1}$ and the irradiation power density was 1 W cm^{-2} . The morphology of SW-1990-LUC and Pan02-luc cells in the different groups was observed. After irradiation for 5 min, typical morphological characteristics of pyroptosis, including cell swelling and the formation of large bulging bubbles on the plasma membrane, were observed in the PTT group, indicating that pyroptotic cell death was triggered by PTT (Fig. S2a, b). Furthermore, real-time morphological tracking of SW-1990-LUC cells was recorded after PTT (Fig. 1a). The pyroptosis index was used to evaluate the dynamic pyroptosis-inducing ability of PTT in vitro [53]. As shown in Fig. 1b, the percentage

of pyroptotic SW-1990-LUC cells significantly increased over time after PTT treatment. To analyse the leakage of intracellular contents, the release of lactate dehydrogenase (LDH) was measured in the SW-1990-LUC and Pan02-luc cell supernatants [54]. As shown in Fig. 1c, LDH release by SW-1990-LUC cells was much greater in the PTT group than in the Blank (25.25% vs. 6.55%; $n=3$; $P<0.0001$) and ICG group (25.25% vs. 8.75%; $n=3$; $P=0.0001$). Similar results were obtained for Pan02-luc cells (Fig. 1d). LDH release was significantly greater in the PTT group than in the Blank (22.81% vs. 4.70%; $n=3$; $P<0.0001$) and ICG group (22.81% vs. 8.24%; $n=3$; $P<0.0001$). According to research on pyroptosis pathways, pyroptosis most commonly occurs through the GSDMD-dependent classical inflammasome pathway and the GSDME-dependent nonclassical pathway [55]. Therefore, we investigated the expression and cleavage of GSDMD and GSDME in PC cell lines after PTT. The levels of GSDMA, GSDMB, GSDMC, GSDMD and GSDME were measured in SW-1990-LUC cells by RT-qPCR, and the expression level of GSDMD was significantly greater than that of GSDMA ($P=0.0002$), GSDMB ($P<0.0001$), GSDMC ($P<0.0001$) and GSDME ($P<0.0001$; Fig. S3). Second, as shown in Fig. 1e and S4, the levels of full-length of GSDMD (GSDMD-FL) and full-length GSDME (GSDME-FL) were measured in SW-1990-LUC cells. The expression level of GSDMD-FL was lower in the PTT group than in the Blank and ICG groups, while the expression level of the cleaved GSDMD (GSDMD-N) was obviously greater in the PTT group. No difference in GSDME-FL expression among the three groups was observed, and the cleaved GSDME (GSDME-N) was not detected (Fig. S4).

GSDMD has been identified as the specific substrate of caspase-1. Western blotting was performed to measure the expression and cleavage of caspase-1. As shown in Fig. 1e, cleaved caspase-1 was detected only in the PTT group, indicating that caspase-1 is cleaved in pancreatic cancer cells after PTT. To further analyse the involvement of caspase-1 in PTT-triggered pyroptosis, VX-765, a caspase-1 specific inhibitor, was applied prior to PTT. As shown in Fig. 1f, g, pretreatment with VX-765 significantly reduced the pyroptosis index 60 min after PTT (79.77% vs. 7.77%, $P=0.0008$).

In the GSDMD-dependent classical inflammasome pathway, cleaved caspase-1 activates not only GSDMD but also the inflammatory cytokines IL-18 and IL-1 β , after which mature IL-18 and IL-1 β are eliminated from cells [56, 57]. Therefore, the levels of mature IL-18 and IL-1 β in the cell supernatant is also an indicator of caspase-1/GSDMD pathway activity. In this study, the concentrations of IL-18 and IL-1 β in the cell supernatant were significantly greater in the PTT group than in the Blank and ICG groups (Fig. 1h, i and S2c, d). These results demonstrate that PTT-triggered pyroptosis is dependent on the caspase-1/GSDMD pathway.

PTT induces pancreatic cancer cell pyroptosis *in vivo*

To analyse the induction of pyroptosis *in vivo*, SW-1990 tumour-bearing mice were divided into Blank, ICG and PTT groups ($n=3$). As shown in Fig. 2a, b and S5, cleaved caspase-1, as well as mature IL-1 β and IL-18, were upregulated in tumour tissues from PTT group compared with those from the Blank and ICG groups. Furthermore, increased expression of GSDMD-N was observed on the cell membrane in the PTT group via immunofluorescence staining (Fig. 2c), confirming that PTT induced pyroptosis *in vivo*.

Tumour-inhibiting effect of PTT *in vivo*

To evaluate the therapeutic effects of PTT in SW-1990-LUC tumour-bearing mice, BALB/c nu/nu mice were divided into Blank, ICG and PTT groups. Tumour weights were recorded ($n=3$), which revealed that the tumour weights in the PTT group at 15 days posttreatment were significantly lower than those in the Blank ($P<0.0001$) and ICG groups ($P<0.0001$). No significant difference was observed between the Blank and ICG groups ($P=0.9644$; Fig. 2d, e). To preliminarily evaluate the toxicity of PTT, the body weights of the mice were monitored ($n=5$). The results revealed that the body weights at 15 days posttreatment were significantly greater in the PTT group than in the Blank ($P=0.0445$) and ICG groups (0.0197) (Fig. 2f), suggesting that PTT, to a certain extent, did not elicit acute or fatal systemic toxicity. Survival analysis ($n=5$) revealed that the overall survival of the mice that received PTT was greater than those of mice in the Blank ($P=0.0018$; $\chi^2=9.701$; DF=1) and ICG groups ($P=0.0018$; $\chi^2=9.701$; DF=1) (Fig. 2g). To further evaluate the antitumour efficacy of PTT, haematoxylin and eosin (H&E) staining was performed, which revealed considerable cellular damage to cancerous tissues in the PTT group (Fig. 2h).

Synergistic therapeutic effect of PTT and a STING agonist as an immune adjuvant

IRF-3 is the main downstream effector of the STING pathway, and phosphorylation of STING-TBK1-IRF3

signaling activated by a STING agonist has been recognized as a promising strategy to enhance antitumour immunity. However, given the complexity of the immune modulation network, caution must be taken with applying synergistic therapies to improve therapeutic outcomes in order to avoid adverse effects. Although PTT can inhibit tumour growth, combined therapies are more effective for increasing treatment efficiency, eliciting a stronger immune response and avoiding adverse effects.

First, we explored whether a STING agonist can enhance PTT-induced pyroptosis *in vitro*. The expression of GSDMD-N, cleaved caspase-3, and phosphorylated-IRF3 (p-IRF3) was measured in the PTT, c-di-GMP and c-di-GMP+PTT groups, and it was found that the expression levels of these proteins were obviously increased in the c-di-GMP+PTT group, as shown in Fig. 3a. According to morphological analysis, more typical morphological characteristics of pyroptosis were observed in the c-di-GMP+PTT group than in the other groups (Fig. 3b). These data reveal that c-di-GMP+PTT triggers pyroptosis via the caspase-1/GSDMD pathway and that a STING agonist can enhance the induction of pyroptosis by PTT.

To investigate whether administration of a STING agonist as an immune adjuvant by intratumoral injection can increase the efficacy of PTT, Pan02-luc cells were subcutaneously injected into C57BL/6 N mice to establish a tumour model, and the mice were divided into the Blank, PTT, c-di-GMP and c-di-GMP+PTT groups (Fig. 3c). The tumour volume was monitored every 2 days. The tumours in the c-di-GMP+PTT group had almost disappeared at 10 days post-treatment. In addition, the tumour volume was significantly reduced in the PTT, c-di-GMP and c-di-GMP+PTT groups compared with the Blank group. Notably, the tumour volume in the c-di-GMP+PTT group was significantly lower than that in the PTT and c-di-GMP groups (PTT vs. c-di-GMP+PTT, $P=0.0006$; c-di-GMP vs. c-di-GMP+PTT, $P=0.0265$; Fig. 3d), indicating a favourable antitumour effect of c-di-GMP+PTT treatment. To assess prognosis and long-term survival, the mice were monitored for 90 days following treatment. As shown in Fig. 3e, the median survival time in the c-di-GMP+PTT group (85 days) was significantly greater than that in the Blank (55 days; $P=0.0018$), PTT (71 days; $P=0.0039$), and c-di-GMP groups (66 days; $P=0.0018$). Most notably, compared with those of the Blank and PTT groups, the median survival rates of the c-di-GMP+PTT group were prolonged by 54.55% and 19.72%, respectively. For the biosafety assay, the body weights of the mice were measured. As shown in Fig. 3f and S6, no body weight loss or abnormal changes in the spleen coefficient were observed between the Blank, PTT, c-di-GMP or c-di-GMP+PTT groups. No high-grade adverse effects were observed

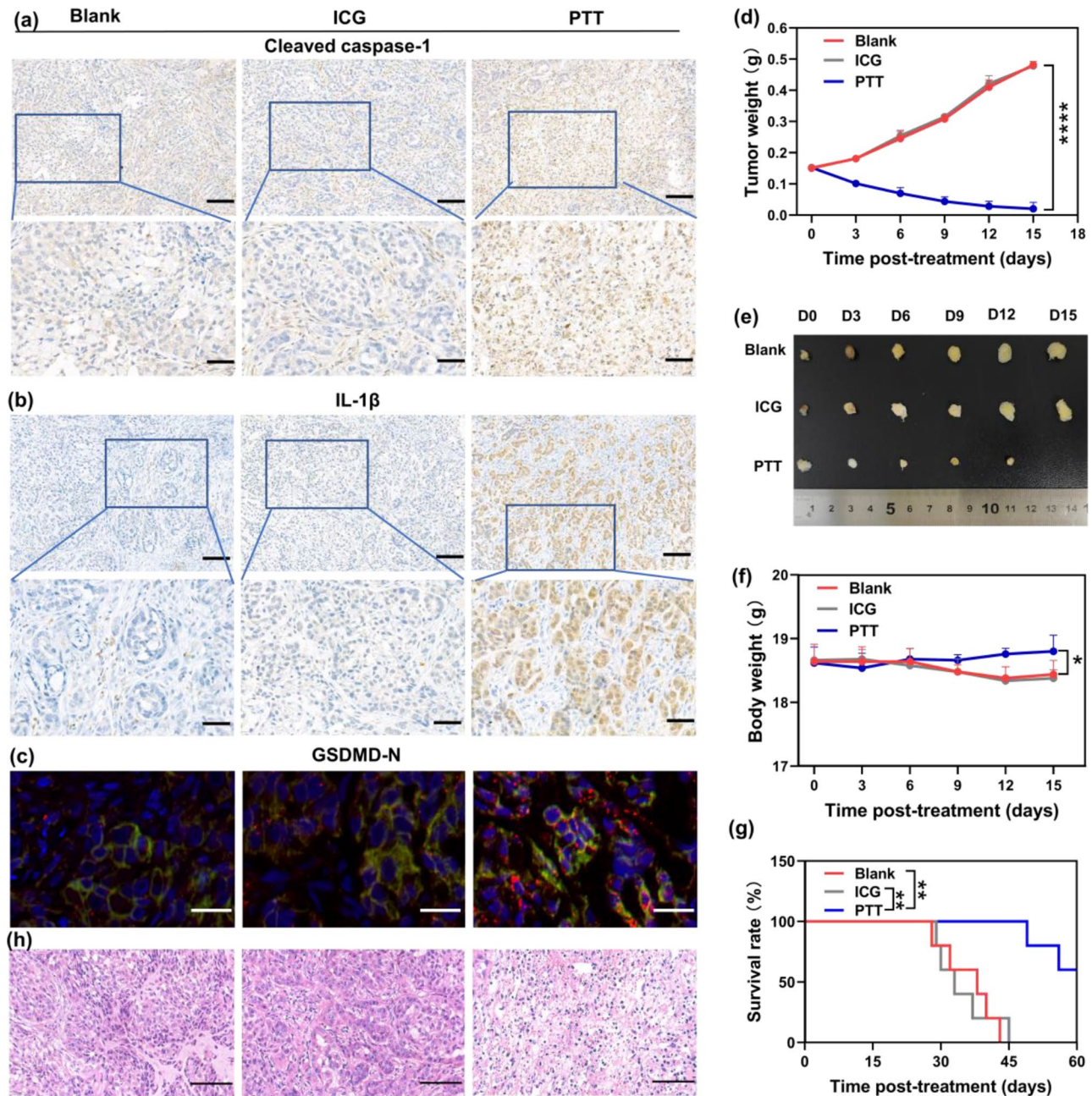


Fig. 2 Pyroptosis induced by PTT in vivo and evaluation of the therapeutic effect in SW-1990-LUC tumour-bearing mouse model. (a and b) Expression of cleaved caspase-1 (a) and mature IL-1 β (b) in tumour tissues detected via immunohistochemical staining. Scale bar: 100 μ m, 50 μ m. (c) Expression of GSDMD-N in tumour tissues examined by immunofluorescence staining. Red, green and blue indicate GSDMD-N, cell membrane and nucleus, respectively. Scale bar: 20 μ m. (d and e) Tumour weights (d) and morphological images (e) at 0, 3, 6, 9, 12, 15 days post PTT ($n=3$). (f) Body weights of mice at 0, 3, 6, 9, 12, 15 days after PTT ($n=5$). (g) Survival analysis of mice during a 60-day observation after PTT ($n=5$). (h) H&E staining of the tumour tissues after treatment. Scale bar: 100 μ m. All the experiments were repeated 3 times independently. For analysis of tumour weight and body weight at 15 days post PTT, data were represented as mean \pm SD if they accord with normal distribution. The comparison among different groups was carried out using one-way ANOVA followed by post hoc test. For survival analysis, Kaplan-Meier survival curves were conducted and the comparison between different groups was performed by Mantel-Cox test. *, $P < 0.05$; **, $P < 0.01$; ****, $P < 0.0001$.

for PTT, c-di-GMP and c-di-GMP + PTT. Next, H&E staining of the major organs was performed, and results indicated the good biocompatibility of c-di-GMP + PTT (Fig. 3g).

Systemic antitumour immunity and immune modulation elicited by PTT and a STING agonist

The application of an appropriate immune adjuvant has been synergistically recognized as a promising strategy

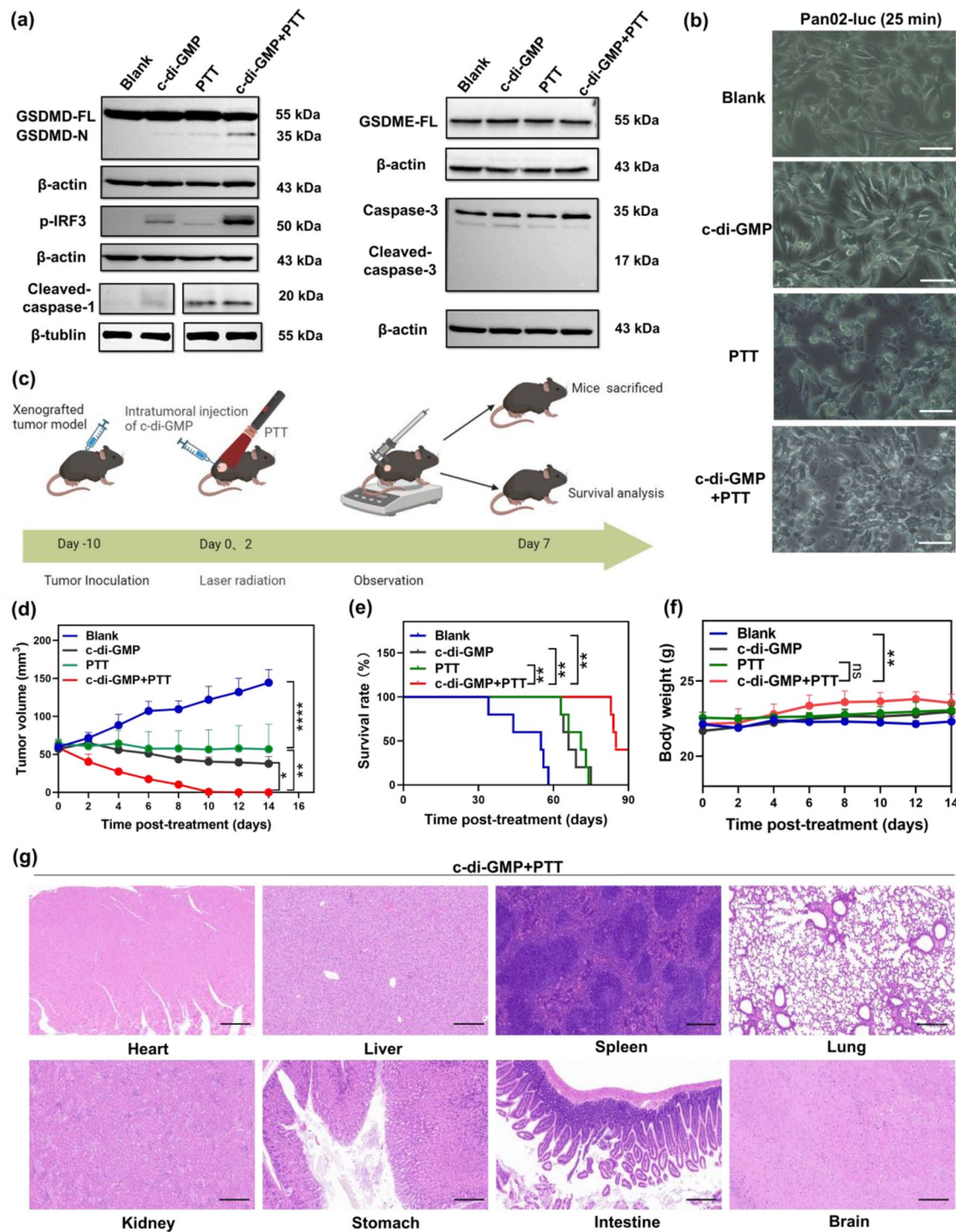


Fig. 3 Pyroptosis induced by PTT combined with STING agonist and evaluation of anti-tumour effects of different therapies in Pan02-luc tumour-bearing mice. **(a)** Pan02-luc cells were divided into the Blank, PTT, c-di-GMP and c-di-GMP + PTT groups. Total proteins were extracted and subjected to western blotting analysis. **(b)** Morphological images of Pan02-luc after different treatments under a bright field microscope. Scale bar: 100 μ m. **(c)** Schematic diagram of the pancreatic tumour model and administration method. **(d)** The tumour volume during a 14-day observation post treatment ($n=5$). **(e)** Survival analysis of mice during a 90-day observation post treatment ($n=5$). **(f)** The body weight of mice during a 14-day observation post treatment ($n=5$). **(g)** H&E staining of the major organs from the c-di-GMP + PTT treated mice. Scale bar: 100 μ m. For analysis of tumour volume and body weight at 14 days post treatment, data were represented as mean \pm SD if they accord with normal distribution. The comparison among different groups was carried out using one-way ANOVA followed by post hoc test. For survival analysis, Kaplan-Meier survival curves were conducted and the comparison between different groups was performed by Mantel-Cox test. *, $P < 0.05$; **, $P < 0.01$; ***, $P < 0.001$; ****, $P < 0.0001$

to enhance PTT-triggered antitumour immunity. To investigate systemic immune responses and changes in the TME in vivo, we established a bilateral flank model of Panc02 tumour in C57BL/6 mice (Fig. S7). As shown in Fig. 4a and b, PTT and the combination therapy not only eradicated the primary tumours but also shrank distant tumours by inducing systemic antitumour immunity. c-di-GMP+PTT treatment led to a complete response in 3 out of 5 mice and prolonged the median survival time to 90 days from 36 days in the Blank group (Blank vs. PTT, $P=0.0018$; PTT vs. c-di-GMP+PTT, $P=0.0316$; Fig. 4c).

Flow cytometry was performed to detect the induced DC maturation and tumour infiltrating T-cell frequencies. Primary tumours and spleens were removed 7 days after the first treatment ($n=3$). The maturity of DCs in the spleen was analysed by assessing CD11c⁺CD86⁺ expression. An increased frequency of mature DCs was detected upon treatment with c-di-GMP+PTT and PTT (Blank vs. PTT, $P=0.0038$; Blank vs. c-di-GMP+PTT, $P=0.0001$; Fig. 4d). After DC maturation, naïve T cells are primed through antigen presentation. We found that compared with Blank group, the frequency of CD3⁺ T cells in primary tumour was greater in the PTT and c-di-GMP+PTT groups than in the Blank group (Fig. S8a), and the frequency of CD3⁺ T cells in the spleen was greater in the c-di-GMP+PTT group ($P=0.0322$; Fig. S8b). The frequencies of CD4⁺ and CD8⁺ T cells in primary tumour were significantly increased in PTT and c-di-GMP+PTT groups when compared to the Blank group (Fig. 4e, f and Fig. S8c). Notably, the frequency of tumour infiltrating immunosuppressive regulatory T (Treg) cells was also decreased in the c-di-GMP+PTT group compared with the Blank group ($P=0.0071$; Fig. 4g). More importantly, compared with PTT alone, the combination therapy increased the frequencies of mature DCs ($P=0.0296$; Fig. 4d) and CD8⁺ T cells ($P=0.0178$; Fig. S8c) in the spleen, and decreased the frequency of Treg cells ($P=0.0496$; Fig. 4g). The presence of mature DCs and increased frequencies of tumour infiltrating T cells indicated that an adaptive immune response was initiated, and antitumour immunity was increased by c-di-GMP+PTT compared with PTT alone. These results demonstrate that a STING agonist could serve as an immune adjuvant to enhance PTT-induced antitumour immunity.

We next examined how PTT reprograms the TME. Immunofluorescence revealed the recruitment of more immunostimulatory M1 macrophages than immunosuppressive M2 macrophages in distant tumours in the PTT and c-di-GMP+PTT groups, as shown by the expression of the M1 marker iNOS, M2 marker CD206 and the macrophage marker F4/80, suggesting a more immunostimulatory TME (Fig. 4h and S9). Masson's trichrome

staining and immunofluorescence staining were also performed to examine the density of intratumoural collagen, a major component of the extracellular matrix (ECM), and α -smooth muscle actin (α -SMA), a microfilament protein used as a marker for activated CAFs (Fig. 4i, j, k). The results showed that c-di-GMP+PTT was more effective than all other treatments in depleting both collagen and CAFs in the tumours, which is likely responsible for reducing tumour stiffness and elasticity, indicating the removal of the physical barrier for T lymphocyte infiltration.

Overexpression of GSDMD may indicate chemotherapy resistance and the potential benefits of local treatment

First, we compared GSDMD expression in pancreatic tumour and normal tissues by analysing gene expression data from the Cancer Genome Atlas (TCGA, <https://portal.gdc.cancer.gov>) and Genotype-Tissue Expression (GTEx, <https://www.gtexportal.org/home/>) databases. As shown in Fig. 5a, GSDMD was significantly upregulated in tumour tissues ($n=178$) compared with normal tissues ($n=167$) according to the Wilcoxon rank-sum test. Notably, in most pancreatic tumour tissues, GSDMD was found to be highly expressed (Fig. 5b). Therefore, the expression of GSDMD could be used to differentiate pancreatic tumour tissues from normal tissues, with an area under the ROC curve (AUC) of 0.91 (Fig. 5c). To further verify whether GSDMD is overexpressed in PC, we analysed 20 paired tumour and normal tissues from surgically resected samples. Consistently, the immunohistochemistry (IHC) results revealed that GSDMD was highly expressed in tumour tissues (Fig. 5d). Next, we analysed the correlation between GSDMD expression levels and the response to five therapeutic agents used clinically to treat PC, namely, 5-fluorouracil, irinotecan, paclitaxel, gemcitabine and cisplatin. As shown in Fig. 5e-h and Fig. S10, GSDMD gene expression was positively correlated with resistance to 5-fluorouracil, irinotecan, paclitaxel, and cisplatin in PC cell lines but was not associated with response to gemcitabine. These results indicate that overexpression of GSDMD in PC may suggest increased resistance to chemotherapy; therefore, local treatments such as PTT might be promising alternative therapeutic options to chemotherapy in patients with GSDMD overexpression. The correlation between GSDMD gene expression and the immune microenvironment score was analysed using the “estimate” package and the CIBERSORT package. As shown in Fig. 5i, j, patients with high GSDMD gene expression had a lower stromal score, greater infiltration of Tregs and activated NK cells, and less monocyte infiltration. In addition, PDOs were established using PC tissues with differential expression of GSDMD confirmed by IHC (Fig. 5k), which were authenticated by H&E and IHC analysis (Fig. 5l).

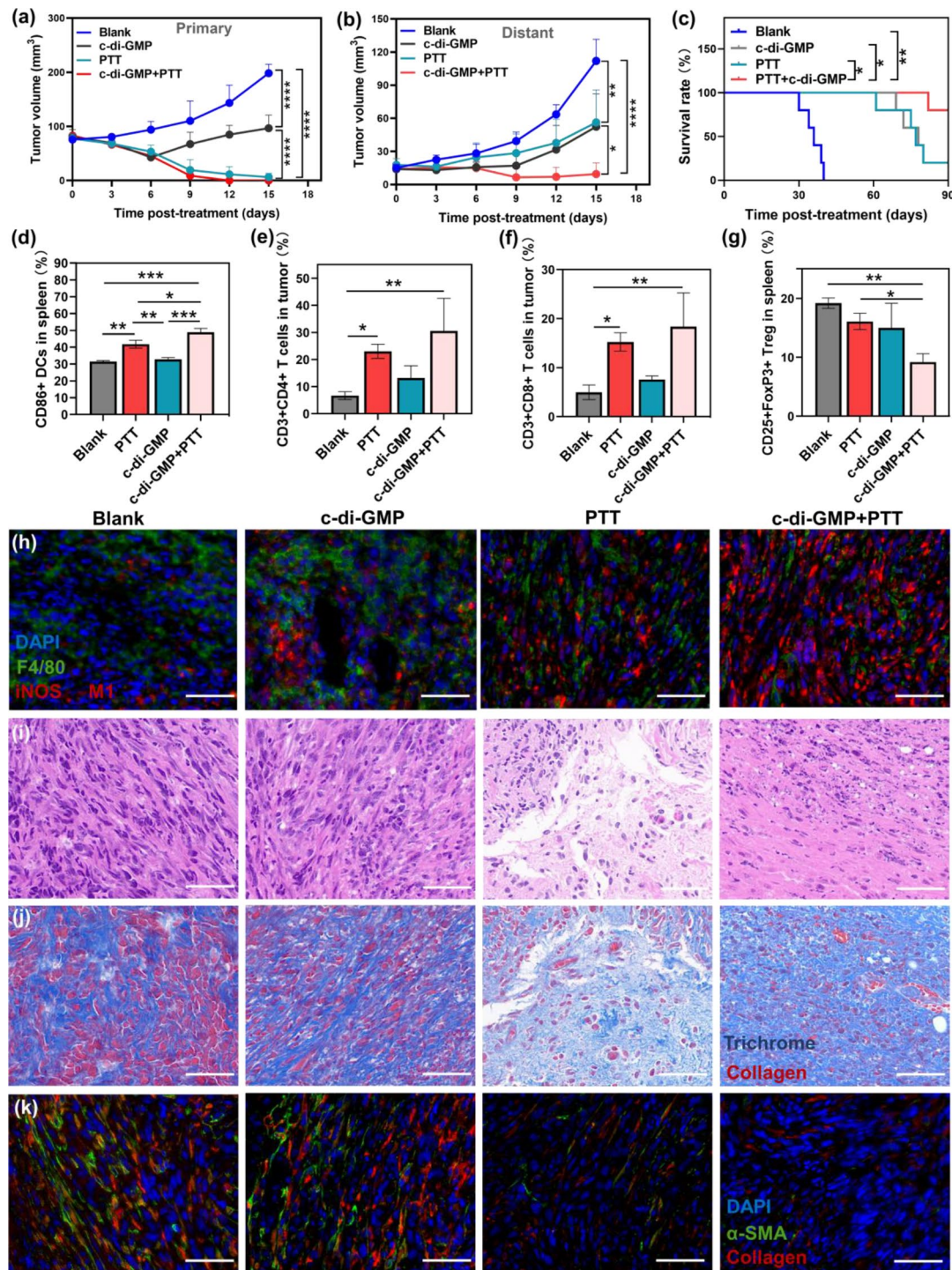


Fig. 4 Evaluation of therapeutic effects and induced systemic antitumour immunity of PTT combined with a STING agonist in a bilateral tumour model. **(a and b)** Tumour volume of the primary and distant tumours during a 15-day observation post treatment ($n=3$). **(c)** Survival analysis of mice during a 90-day observation post treatment ($n=5$). **(d)** Detection of mature DCs in the spleen which were recognized as CD11c⁺CD86⁺. **(e)** Detection of CD4⁺ T cells in primary tumour which were recognized as CD45⁺CD3⁺CD4⁺. **(f)** Detection of CD8⁺ T cells in primary tumour which were recognized as CD45⁺CD3⁺CD8⁺. **(g)** Detection of regulatory T cells (Treg) in the spleen which were recognized as CD45⁺CD4⁺CD25⁺FoxP3⁺. Data were represented as mean \pm SD ($n=3$) if they accord with normal distribution. The comparison among different groups was carried out using one-way ANOVA followed by post hoc test. *, $P<0.05$; **, $P<0.01$; ***, $P<0.001$. **(h)** Immunofluorescence staining of M0 (F4/80) and M1 (iNOS) in distant tumours. Blue, green and red fluorescence indicate nuclei, F4/80 and iNOS, respectively. Scale bar: 50 μ m. **(i and j)** H&E staining and trichrome immunohistochemistry of as-treated tumours for staining of intratumoural collagen. **(k)** Immunofluorescence staining of CAFs and collagen. Blue, green and red fluorescence indicate nuclei, α -SMA and collagen, respectively. Scale bar: 50 μ m

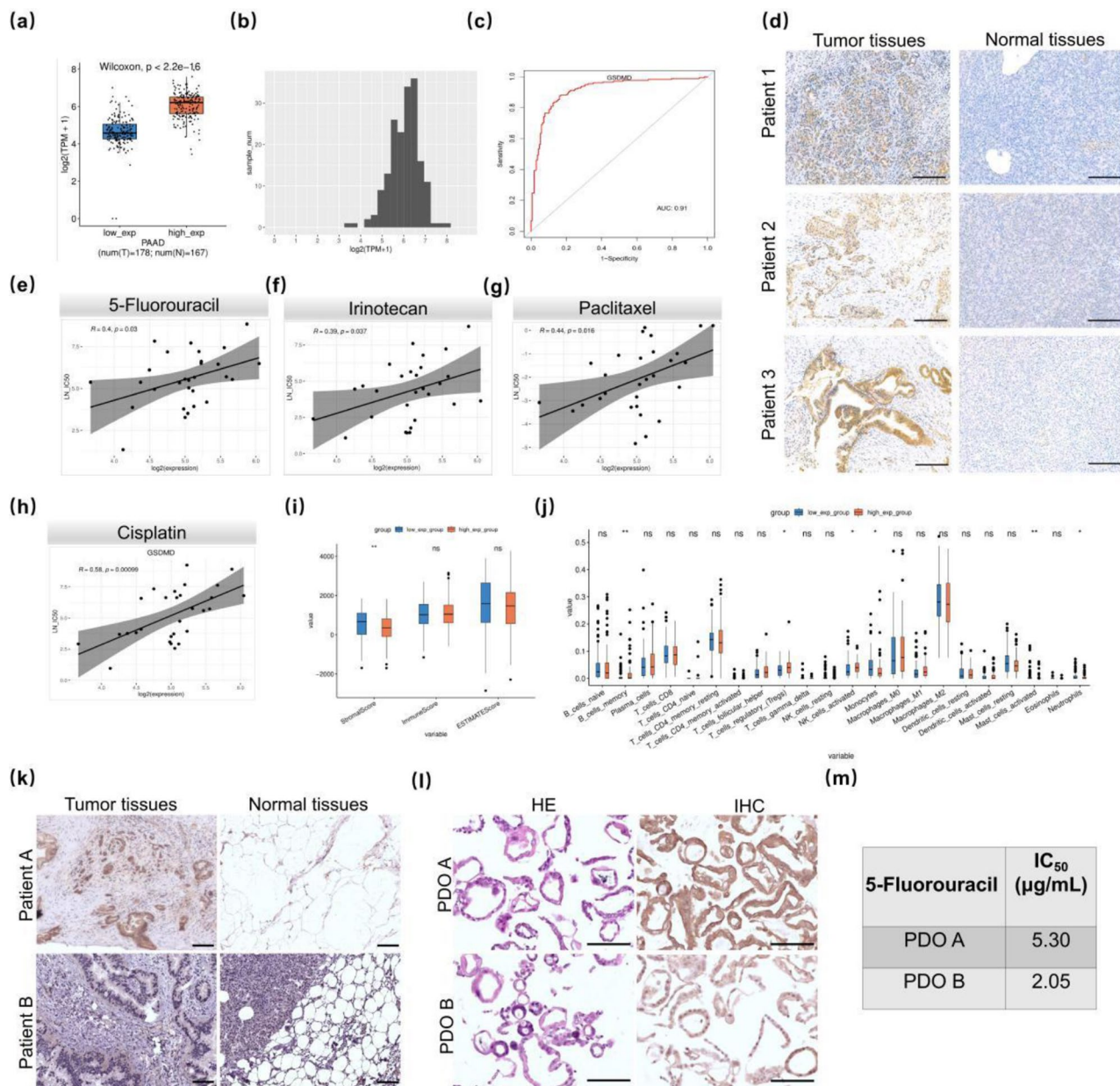


Fig. 5 Aberrant expression and functional implications of GSDMD in PC. **(a)** GSDMD expression in pancreatic tumour tissues (left) and normal tissues (right). **(b)** GSDMD expression in pancreatic tumour tissues. **(c)** The ROC curve of tumour tissues ($n = 178$) and normal tissues ($n = 167$). **(d)** IHC staining of GSDMD in three paired specimens of PC patients. Scale bar: 200 μm . **(e-h)** Drug resistance analysis. The higher the GSDMD expression, the lower the sensitivity to the drug. **(i)** Display information on immune microenvironment score. **(j)** Immune cell infiltration. The horizontal axis represents the 22 immune fractions analysed by cibersort and the vertical axis represents the relative proportions of the immune fractions (the relative proportions of all 22 immune fractions sum to 1) *, $P < 0.05$; **, $P < 0.01$. **(k)** IHC analysis of tumour and normal tissues using antibody against GSDMD. Scale bar: 100 μm . **(l)** H&E staining and IHC analysis using antibody against GSDMD in PDOs. Scale bar: 100 μm . **(m)** Drug sensitivity to 5-fluorouracil in PDOs, with IC_{50} as the indicator

Sensitivity to 5-fluorouracil was assessed, and a higher IC₅₀ was detected for PDO A, which had higher expression of GSDMD (Fig. 5m).

In summary, GSDMD overexpression might be a valuable biomarker for identifying PC patients who may benefit more from local treatment, such as PTT, than chemotherapy.

Discussion

PTT is a promising strategy for treating PC, and the fact that relatively mild temperatures are used during the application of PTT means that severe damage to surrounding normal tissues is prevented. Recently, several studies have reported that PTT can induce an antitumour immune response to eradicate primary and distant tumours [14, 47]. Wang et al. designed an

immunotherapeutic hydrogel that enhances the immune response via PTT-induced ICD and therefore increases the frequencies of mature CD86⁺ DCs and infiltrating NK cells and the M1/M2 macrophage ratio to prevent tumour metastasis [14]. Furthermore, it has also been reported that photodynamic therapy (PDT)-triggered pyroptosis induces antitumour immunity in PC [47]. However, whether PTT can induce pyroptosis in PC and the underlying mechanism remain unknown. In this study, we demonstrated that PTT can cause pyroptosis in a certain percentage of PC cells via a GSDMD-dependent pathway and therefore elicit antitumour immunity through the release of various inflammatory cytokines (such as IL-1 β), which promotes the maturation of DCs, facilitates antigen presentation to CD4⁺ T cells, increases the frequency of tumour-specific CD8⁺ T cells, and converts immunosuppressive M2 macrophages to immunostimulatory M1 macrophages in the TME.

STING agonists can increase tumour immunogenicity and elicit robust antitumour immune responses, making them particularly attractive for treating PC [58–62]. STING is widely expressed in multiple cell types in the TME and has a unique ability to achieve a balance between the secretion of proinflammatory cytokines and the secretion of type I IFNs to activate DCs and increase the frequency of CD8⁺ T cells [45, 63, 64]. Since cGAS recognizes DNA of a certain length without sequence specificity, DNA of any origin can elicit an immune response through activation of the cGAS-STING pathway. Abe et al. [65] reported that STING colocalizes with DNA intracellularly and binds to dsDNA and single-stranded DNA (ssDNA). As a type of cell death, pyroptosis can cause the release of damaged DNA, which can activate the STING pathway [43]. Yang et al. reported that STING induces pyroptosis in primary murine hepatocytes by activating the NLRP3 inflammasome and that STING knockout ameliorates hepatic pyroptosis [49]. Moreover, recent studies have shown that PDT and PTT can disrupt the intracellular redox balance, leading to mitochondrial or nuclear DNA damage and even the leakage of mitochondrial or nuclear DNA into the cytoplasm, thus activating the cGAS-STING signalling pathway and inducing antitumour immune response while exerting fewer toxic side effects [46, 66–69]. Direct pharmacological activation of STING with a STING agonist has emerged as a new type immunotherapy strategy for cancer [70, 71]. In this study, the STING agonist c-di-GMP was used as an immune adjuvant, and the combined therapy increased the tumour inhibition rate, prolonged survival and amplified antitumour immune responses *in vivo*. However, the interactions between STING and the pyroptosis pathway remain to be further clarified.

The route of administration of STING agonists is also very important for determining the efficacy of treatment. Systemic administration of small structural STING agonists inevitably has limited therapeutic effects due to insufficient accumulation in tumours, rapid clearance, a short effective duration and the dense stroma of PC. Therefore, in this study, a STING agonist was administered via intratumoural injection to ensure its direct delivery to the tumour while limiting autoimmune, immunopathological and potential high-grade adverse systemic effects. In addition, reduced tumour stiffness and elasticity due to the depletion of both collagen and CAFs were found in PC tissues after PTT, which may have facilitated the delivery of the drug after injection.

Tumour-associated macrophages (TAMs) play a key role in progression to high-grade (HG) lesions with a cancerous invasive phenotype and an immunosuppressive microenvironment in PC. Macrophages can be polarized to the proinflammatory M1 phenotype or the anti-inflammatory M2 phenotype [72]. Animal studies suggest that M1-like TAMs are involved in tumour rejection by releasing proinflammatory cytokines and promoting Th1 responses, whereas M2-like TAMs promote the remodelling of tissue, the generation of an immunosuppressive environment, tumour growth and metastasis [73–75]. In this study, we explored changes in the TME in local tumours. Upon treatment with PTT alone or in combination with a STING agonist, a robust abscopal effect and systemic immune response were induced via the conversion of M2 macrophages to M1 macrophages, downregulation of collagen expression and inactivation of CAFs. However, this study also has several limitations. Although we explored the phenotypic conversion of macrophages in the TME, whether macrophages of other phenotypes exist and their roles were not studied. Additionally, the mechanisms by which STING agonists enhance PTT-elicited immunity require further investigation.

Additionally, in this study, bioinformatic analysis was performed; the results indicated that GSDMD was highly expressed in PC and the high GSDMD expression correlated with decreased chemosensitivity and the presence of an inhibitory immune microenvironment. IHC staining of surgically resected human samples and analyses of the drug sensitivity of PDOs were carried out, and the bioinformatic data were validated. These results further demonstrate the importance of PTT as a therapeutic modality in the clinic and confirm that GSDMD can be used as a biomarker to identify patients suitable for local PTT.

Owing to the limited penetration depth of the laser, our team first proposed interventional PTT (IPTT) as a minimally invasive treatment method for deeply buried PC in the abdomen [13]. STING agonists can also be injected locally through the needle used for IPTT; thus, IPTT

combined with a STING agonist as an immune adjuvant is a potential treatment of PC.

In summary, PTT can induce pyroptosis via the GSDMD-dependent canonical inflammasome pathway, which can promote systemic antitumoural immunity and cause favourable alterations in the TME in PC. GSDMD can be used as a new biomarker to identify PC patients who may benefit from local PTT treatment. More importantly, a STING agonist synergistically enhanced the therapeutic efficacy of PTT. ICG has already been approved for clinical use, and the local injection of c-di-GMP without other components is relatively safe. Our study indicates that the combination of PTT and STING agonist treatment has great translational value for the treatment of PC and could also be used to treat other cancers.

Supplementary Information

The online version contains supplementary material available at <https://doi.org/10.1186/s12967-025-06247-2>.

Supplementary Material 1

Acknowledgements

Not applicable.

Author contributions

All authors read and approved the final version of the manuscript. Conception and design: Y.Y.H., W.H.X. and X.L.Y. Development of methodology: L.P., J.W.Y., E.P.Q., C.Y., N.G., Z.G.C., H.X.Z. and F.Y.L. E.P.Q., C.Y., Y.Y.H., X.L., Q.W. and N.G. performed the experiments and analysed the results. Y.Y.H., X.L. and J.W.Y. wrote the manuscript, and all other authors revised the manuscript. Study supervision: W.H.X. and X.L.Y. All authors read and approved the final manuscript.

Funding

Not applicable.

Data availability

The method section describes all the data utilized for analysis and processing in this study. On reasonable request, the corresponding author will provide the data and code conclusions of this work.

Declarations

Ethics approval and consent to participate

All animal experiments were approved by the Animal Ethics Committee of Chinese PLA General Hospital and were carried out in compliance with the Animal Management Rules of the Ministry of Health of the People's Republic of China (Document NO.55, 2001). Studies involving human samples were conducted in accordance to recognized ethical guidelines (Declaration of Helsinki) and approved by the Ethics Committee of the Fourth Medical Center of Chinese PLA General Hospital (Document NO. 2024KY045-KS001) with written informed consent.

Consent for publication

This study was approved by the Ethics Committee of the Fourth Medical Center of Chinese PLA General Hospital (Document NO. 2024KY045-KS001) with written informed consent.

Competing interests

The authors declare that they have no competing interests.

Author details

¹Department of Oncology, Senior Department of Oncology, the Fifth Medical Center of PLA General Hospital, Beijing, China

²Department of Interventional Ultrasound, Senior Department of Oncology, The Fifth Medical Center of PLA General Hospital, Beijing 100071, China

³Specialty in Oncology, Jinzhou Medical University, Jinzhou, China

⁴Department of Urology, Addenbrooke's Hospital, Cambridge University Hospitals NHS Foundation, Cambridge, UK

⁵Department of Ultrasound, the Fourth Medical Center of PLA General Hospital, Beijing, China

Received: 2 October 2024 / Accepted: 11 February 2025

Published online: 04 March 2025

References

1. Rahib L, Smith BD, Aizenberg R, Rosenzweig AB, Fleshman JM, Matrisian LM. Projecting cancer incidence and deaths to 2030: the unexpected burden of thyroid, liver, and pancreas cancers in the United States. *Cancer Res*. 2014;74(11):2913–21.
2. Halbrook CJ, Lyssiotis CA, Pasca di Magliano M, Maitra A. Pancreatic cancer: advances and challenges. *Cell*. 2023;186(8):1729–54.
3. Schizas D, Charalampakis N, Kole C, Economopoulou P, Koustas E, Gkotsis E, et al. Immunotherapy for pancreatic cancer: a 2020 update. *Cancer Treat Rev*. 2020;86:102016.
4. Brahmer JR, Tykodi SS, Chow LQ, Hwu WJ, Topalian SL, Hwu P, et al. Safety and activity of anti-PD-L1 antibody in patients with advanced cancer. *N Engl J Med*. 2012;366(26):2455–65.
5. Beatty GL, Haas AR, Maus MV, Torigian DA, Soulen MC, Plesa G, et al. Mesothelin-specific chimeric antigen receptor mRNA-engineered T cells induce anti-tumor activity in solid malignancies. *Cancer Immunol Res*. 2014;2(2):112–20.
6. Le DT, Wang-Gillam A, Picozzi V, Greten TF, Crocenzi T, Springett G, et al. Safety and survival with GVAX pancreas prime and Listeria Monocytogenes-expressing mesothelin (CRS-207) boost vaccines for metastatic pancreatic cancer. *J Clin Oncol*. 2015;33(12):1325–33.
7. Marabelle A, Le DT, Ascierto PA, Di Giacomo AM, De Jesus-Acosta A, Delord JP, et al. Efficacy of Pembrolizumab in patients with Noncolorectal high micro-satellite Instability/Mismatch repair-deficient Cancer: results from the phase II KEYNOTE-158 study. *J Clin Oncol*. 2020;38(1):1–10.
8. Principe DR, Korc M, Kamath SD, Munshi HG, Rana A. Trials and tribulations of pancreatic cancer immunotherapy. *Cancer Lett*. 2021;504:1–14.
9. Flemming A. Cancer: vaccine cure for prostate cancer? *Nat Rev Drug Discov*. 2011;10(8):575.
10. Liu S, Jiang Q, Zhao X, Zhao R, Wang Y, Wang Y, et al. A DNA nanodevice-based vaccine for cancer immunotherapy. *Nat Mater*. 2021;20(3):421–30.
11. Morotti M, Albukhari A, Alsaadi A, Artibani M, Brenton JD, Curbishley SM, et al. Promises and challenges of adoptive T-cell therapies for solid tumours. *Br J Cancer*. 2021;124(11):1759–76.
12. Zhi D, Yang T, O'Hagan J, Zhang S, Donnelly RF. Photothermal therapy. *J Control Release*. 2020;325:52–71.
13. Hu Y, Chi C, Wang S, Wang L, Liang P, Liu F et al. A comparative study of clinical intervention and interventional Photothermal Therapy for Pancreatic Cancer. *Adv Mater* 2017; 29(33).
14. Wang M, Zhang X, Liu B, Liu C, Song C, Chen Y et al. Immunotherapeutic hydrogel with Photothermal Induced Immunogenic Cell Death and STING activation for post-surgical treatment. *Adv Funct Mater* 2023; 33(29).
15. Xu P, Liang F. Nanomaterial-based Tumor Photothermal Immunotherapy. *Int J Nanomed*. 2020;15:9159–80.
16. Luo L, Qin B, Jiang M, Xie L, Luo Z, Guo X, et al. Regulating immune memory and reversing tumor thermotolerance through a step-by-step starving-photothermal therapy. *J Nanobiotechnol*. 2021;19(1):297.
17. Yu P, Zhang X, Liu N, Tang L, Peng C, Chen X. Pyroptosis: mechanisms and diseases. *Signal Transduct Target Ther*. 2021;6(1):128.
18. Du T, Gao J, Li P, Wang Y, Qi Q, Liu X, et al. Pyroptosis, metabolism, and tumor immune microenvironment. *Clin Transl Med*. 2021;11(8):e492.
19. Tan Y, Chen Q, Li X, Zeng Z, Xiong W, Li G, et al. Pyroptosis: a new paradigm of cell death for fighting against cancer. *J Exp Clin Cancer Res*. 2021;40(1):153.
20. Shi J, Gao W, Shao F. Pyroptosis. Gasdermin-mediated programmed necrotic cell death. *Trends Biochem Sci*. 2017;42(4):245–54.

21. Li L, Tian H, Zhang Z, Ding N, He K, Lu S, et al. Carrier-Free Nanoplatfom via evoking pyroptosis and Immune response against breast Cancer. *ACS Appl Mater Interfaces*. 2023;15(1):452–68.
22. Man SM, Karki R, Kanneganti TD. Molecular mechanisms and functions of pyroptosis, inflammatory caspases and inflammasomes in infectious diseases. *Immunol Rev*. 2017;277(1):61–75.
23. Takeuchi O, Akira S. Pattern recognition receptors and inflammation. *Cell*. 2010;140(6):805–20.
24. Fang Y, Tian S, Pan Y, Li W, Wang Q, Tang Y, et al. Pyroptosis: a new frontier in cancer. *Biomed Pharmacother*. 2020;121:109595.
25. de Vasconcelos NM, Lamkanfi M. Recent insights on inflammasomes, Gasdermin Pores, and Pyroptosis. *Cold Spring Harb Perspect Biol*. 2020;12(5).
26. Vanaja SK, Rathinam VA, Fitzgerald KA. Mechanisms of inflammasome activation: recent advances and novel insights. *Trends Cell Biol*. 2015;25(5):308–15.
27. Broz P, Pelegrin P, Shao F. The gasdermins, a protein family executing cell death and inflammation. *Nat Rev Immunol*. 2020;20(3):143–57.
28. Kovacs SB, Miao EA, Gasdermins. Effectors of Pyroptosis. *Trends Cell Biol*. 2017;27(9):673–84.
29. Xu YJ, Zheng L, Hu YW, Wang Q. Pyroptosis and its relationship to atherosclerosis. *Clin Chim Acta*. 2018;476:28–37.
30. Kolb R, Liu GH, Janowski AM, Sutterwala FS, Zhang W. Inflammasomes in cancer: a double-edged sword. *Protein Cell*. 2014;5(1):12–20.
31. Thi HTH, Hong S. Inflammasome as a therapeutic target for Cancer Prevention and Treatment. *J Cancer Prev*. 2017;22(2):62–73.
32. Rathinam VA, Vanaja SK, Fitzgerald KA. Regulation of inflammasome signaling. *Nat Immunol*. 2012;13(4):333–42.
33. Martinon F, Burns K, Tschopp J. The inflammasome: a molecular platform triggering activation of inflammatory caspases and processing of proIL-beta. *Mol Cell*. 2002;10(2):417–26.
34. Lamkanfi M, Dixit VM. Mechanisms and functions of inflammasomes. *Cell*. 2014;157(5):1013–22.
35. Huang Y, Xu W, Zhou R. NLRP3 inflammasome activation and cell death. *Cell Mol Immunol*. 2021;18(9):2114–27.
36. Ramos-Junior ES, Morandini AC, Gasdermin. A new player to the inflammasome game. *Biomed J*. 2017;40(6):313–6.
37. Kayagaki N, Lee BL, Stowe IB, Kornfeld OS, O'Rourke K, Mirrashidi KM et al. IRF2 transcriptionally induces GSDMD expression for pyroptosis. *Sci Signal*. 2019;12(582).
38. Li S, Yue M, Xu H, Zhang X, Mao T, Quan M, et al. Chemotherapeutic drugs-induced pyroptosis mediated by gasdermin E promotes the progression and chemoresistance of pancreatic cancer. *Cancer Lett*. 2023;564:216206.
39. Bao Y, Ge Y, Wu M, Mao Z, Ye J, Tong W. Record-High Ultrasound-Sensitive NO Nanogenerators for Cascade Tumor Pyroptosis and Immunotherapy. *Advanced Science*. 2023;10(26).
40. Garland KM, Sheehy TL, Wilson JT. Chemical and Biomolecular strategies for STING pathway activation in Cancer Immunotherapy. *Chem Rev*. 2022;122(6):5977–6039.
41. Wang Y, Luo J, Alu A, Han X, Wei Y, Wei X. cGAS-STING pathway in cancer biotherapy. *Mol Cancer*. 2020;19(1):136.
42. Qu J, Cai Y, Li F, Li X, Liu R. Potential therapeutic strategies for colitis and colon cancer: bidirectional targeting STING pathway. *EBioMedicine*. 2024;111:105491.
43. Fan X, Song X, Chen W, Liang H, Nakatsukasa H, Zhang D. cGAS-STING signaling in cancer: regulation and therapeutic targeting. *MedComm—Oncol*. 2023;2(3).
44. Cheng N, Watkins-Schulz R, Junkins RD, David CN, Johnson BM, Montgomery SA et al. A nanoparticle-incorporated STING activator enhances antitumor immunity in PD-L1-insensitive models of triple-negative breast cancer. *JCI Insight*. 2018;3(22).
45. Motwani M, Pesiridis S, Fitzgerald KA. DNA sensing by the cGAS-STING pathway in health and disease. *Nat Rev Genet*. 2019;20(11):657–74.
46. Sun X, Zhang S, Li Q, Yang M, Qiu X, Yu B, et al. Bimetallic infinite coordination nanopolymers via phototherapy and STING activation for eliciting robust antitumor immunity. *J Colloid Interface Sci*. 2023;642:691–704.
47. Wang M, Wu M, Liu X, Shao S, Huang J, Liu B, et al. Pyroptosis remodeling Tumor Microenvironment to Enhance Pancreatic Cancer Immunotherapy driven by membrane anchoring Photosensitizer. *Adv Sci (Weinh)*. 2022;9(29):e2202914.
48. Ling YY, Xia XY, Hao L, Wang WJ, Zhang H, Liu LY, et al. Simultaneous photoactivation of cGAS-STING pathway and pyroptosis by platinum(II) triphenylamine complexes for Cancer Immunotherapy. *Angew Chem Int Ed Engl*. 2022;61(43):e202210988.
49. Xiao Y, Zhao C, Tai Y, Li B, Lan T, Lai E, et al. STING mediates hepatocyte pyroptosis in liver fibrosis by Epigenetically activating the NLRP3 inflammasome. *Redox Biol*. 2023;62:102691.
50. Peng Y, Yang Y, Li Y, Shi T, Xu N, Liu R, et al. Mitochondrial (mt)DNA-cyclic GMP-AMP synthase (cGAS)-stimulator of interferon genes (STING) signaling promotes pyroptosis of macrophages via interferon regulatory factor (IRF)7/IRF3 activation to aggravate lung injury during severe acute pancreatitis. *Cell Mol Biol Lett*. 2024;29(1):61.
51. Wu JJ, Zhao L, Hu HG, Li WH, Li YM. Agonists and inhibitors of the STING pathway: potential agents for immunotherapy. *Med Res Rev*. 2020;40(3):1117–41.
52. Ding C, Song Z, Shen A, Chen T, Zhang A. Small molecules targeting the innate immune cGAS-STING-TBK1 signaling pathway. *Acta Pharm Sin B*. 2020;10(12):2272–98.
53. Xiao Y, Zhang T, Ma X, Yang QC, Yang LL, Yang SC, et al. Microenvironment-responsive Prodrug-Induced pyroptosis boosts Cancer Immunotherapy. *Adv Sci (Weinh)*. 2021;8(24):e2101840.
54. Fan JX, Deng RH, Wang H, Liu XH, Wang XN, Qin R, et al. Epigenetics-based Tumor cells pyroptosis for enhancing the Immunological Effect of Chemotherapeutic Nanocarriers. *Nano Lett*. 2019;19(11):8049–58.
55. Tong X, Tang R, Xiao M, Xu J, Wang W, Zhang B, et al. Targeting cell death pathways for cancer therapy: recent developments in necroptosis, pyroptosis, ferroptosis, and cuproptosis research. *J Hematol Oncol*. 2022;15(1):174.
56. Wang Y, Gao W, Shi X, Ding J, Liu W, He H, et al. Chemotherapy drugs induce pyroptosis through caspase-3 cleavage of a gasdermin. *Nature*. 2017;547(7661):99–103.
57. Wu M, Liu X, Chen H, Duan Y, Liu J, Pan Y, et al. Activation of pyroptosis by membrane-anchoring AIE Photosensitizer Design: New Prospect for Photodynamic Cancer cell ablation. *Angew Chem Int Ed Engl*. 2021;60(16):9093–8.
58. Li X, Khorsandi S, Wang Y, Santelli J, Huntoon K, Nguyen N, et al. Cancer immunotherapy based on image-guided STING activation by nucleotide nanocomplex-decorated ultrasound microbubbles. *Nat Nanotechnol*. 2022;17(8):891–9.
59. Zaver SA, Woodward JJ. Cyclic dinucleotides at the forefront of innate immunity. *Curr Opin Cell Biol*. 2020;63:49–56.
60. Corrales L, Glickman LH, McWhirter SM, Kanne DB, Sivick KE, Katibah GE, et al. Direct activation of STING in the Tumor Microenvironment leads to potent and systemic Tumor regression and immunity. *Cell Rep*. 2015;11(7):1018–30.
61. Su T, Zhang Y, Valerie K, Wang XY, Lin S, Zhu G. STING activation in cancer immunotherapy. *Theranostics*. 2019;9(25):7759–71.
62. Ishikawa H, Barber GN. STING is an endoplasmic reticulum adaptor that facilitates innate immune signalling. *Nature*. 2008;455(7213):674–8.
63. Woo SR, Fuertes MB, Corrales L, Spranger S, Furdyna MJ, Leung MY, et al. STING-dependent cytosolic DNA sensing mediates innate immune recognition of immunogenic tumors. *Immunity*. 2014;41(5):830–42.
64. Zitvogel L, Galluzzi L, Kepp O, Smyth MJ, Kroemer G. Type I interferons in anticancer immunity. *Nat Rev Immunol*. 2015;15(7):405–14.
65. Abe T, Harashima A, Xia T, Konno H, Konno K, Morales A, et al. STING recognition of cytoplasmic DNA instigates cellular defense. *Mol Cell*. 2013;50(1):5–15.
66. Song W, Song SJ, Kuang J, Yang H, Yu T, Yang F, et al. Activating Innate immunity by a STING Signal Amplifier for local and systemic immunotherapy. *ACS Nano*. 2022;16(10):15977–93.
67. Wang K, Li Y, Wang X, Zhang Z, Cao L, Fan X, et al. Gas therapy potentiates aggregation-induced emission luminogen-based photoimmunotherapy of poorly immunogenic tumors through cGAS-STING pathway activation. *Nat Commun*. 2023;14(1):2950.
68. Xia J, Wang L, Shen T, Li P, Zhu P, Xie S, et al. Integrated manganese (III)-doped nanosystem for optimizing photothermal ablation: amplifying hyperthermia-induced STING pathway and enhancing antitumor immunity. *Acta Biomater*. 2023;155:601–17.
69. Zhang Y, Li Z, Milon Essola J, Ge K, Dai X, He H, et al. Biosafety materials: ushering in a new era of infectious disease diagnosis and treatment with the CRISPR/Cas system. *Biosaf Health*. 2022;4(2):70–8.
70. Yang J, Guo W, Huang R, Bian J, Zhang S, Wei T, et al. Self-assembled albumin nanoparticles induce pyroptosis for photodynamic/photothermal/immuno synergistic therapies in triple-negative breast cancer. *Front Immunol*. 2023;14:1173487.
71. Yu X, Yu J, Dai H, Deng C, Sun X, Long S, et al. Novel formulation of c-di-GMP with cytidinyl/cationic lipid reverses T cell exhaustion and activates stronger anti-tumor immunity. *Theranostics*. 2022;12(15):6723–39.
72. Liou GY, Bastea L, Fleming A, Doppler H, Edenfield BH, Dawson DW, et al. The Presence of Interleukin-13 at pancreatic ADM/PanIN lesions alters

- macrophage populations and mediates pancreatic tumorigenesis. *Cell Rep.* 2017;19(7):1322–33.
73. Storz P. Roles of differently polarized macrophages in the initiation and progression of pancreatic cancer. *Front Immunol.* 2023;14:1237711.
74. Jaynes JM, Sable R, Ronzetti M, Bautista W, Knotts Z, Abisoye-Ogunniyan A et al. Mannose receptor (CD206) activation in tumor-associated macrophages enhances adaptive and innate antitumor immune responses. *Science translational medicine* 2020; 12(530).
75. Mantovani A, Marchesi F, Malesci A, Laghi L, Allavena P. Tumour-associated macrophages as treatment targets in oncology. *Nat Rev Clin Oncol.* 2017;14(7):399–416.

Publisher's note

Springer Nature remains neutral with regard to jurisdictional claims in published maps and institutional affiliations.